Full Paper

Journal of the Brazilian Chemical Society

https://dx.doi.org/10.21577/0103-5053.20260078

*J. Braz. Chem. Soc.* **2026**, *37-Spe1*, e-20260078, 1-19


# Molecular Networking-Based Annotation of Alkaloids in Methanolic Extracts of Amaryllidaceae Species and Evaluation of Their Antileishmanial Activity

*Amanda E. Feu,[a] Marcos V. V. Lyrio,[b] Lays Rafalscky,[b] Bruno A. Lessa,[b] Marilú R. Soto-Vásquez,[c] Thalita B. Riul,[d] Jean P. de Andrade,[e] Wanderson Romão*[,b,f] and Warley S. Borges*[,b]*

[a]*Instituto Federal de Educação, Ciência e Tecnologia do Espírito Santo (IFES), 29040-780 Vitória-ES, Brazil*

[b]*Universidade Federal do Espírito Santo (UFES), 29075-910 Vitória-ES, Brazil*

[c]*Facultad de Farmacia y Bioquímica, Universidad Nacional de Trujillo, Trujillo, Peru*

[d]*Faculdade de Ciências Farmacêuticas, Alimentos e Nutrição, Universidade Federal de Mato Grosso do Sul, 79070-900 Campo Grande-MS, Brazil*

[e]*Departamento de Medicina Traslacional, Facultad de Medicina, Universidad Católica del Maule, 3480112 Talca, Chile*

[f]*Instituto Federal de Educação, Ciência e Tecnologia do Espírito Santo (IFES), 29106-010 Vila Velha-ES, Brazil*

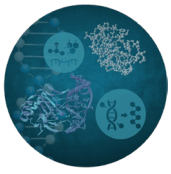

The Amaryllidaceae family is widely recognized for its remarkable alkaloid diversity, comprising secondary metabolites with significant pharmacological potential. Advances in liquid chromatography-mass spectrometry (LC-MS) combined with molecular networking strategies have enabled comprehensive structural characterization and visualization of complex metabolite datasets. Considering the limited efficacy and toxicity associated with current therapies for leishmaniasis, a neglected tropical disease of global relevance, Amaryllidaceae species represent a promising source of novel antileishmanial compounds. This study investigated the alkaloid diversity of methanolic extracts obtained from bulbs of 52 wild and hybrid Amaryllidaceae species collected in Latin American countries and evaluated their activity against *Leishmania amazonensis*. Extracts were analyzed by LC-MS and processed using MZmine, followed by feature-based molecular networkin (FBMN). This workflow enabled the annotation of 28 alkaloids organized into structurally related clusters, in addition to more than 15 compounds detected as unique nodes based on spectral similarity. Biological assays against promastigote forms, together with cytotoxicity evaluation in NIH/3T3 cells, identified *Ismene amancaes* as the most active extract (half-maximal inhibitory concentration ($IC_{50}$) = 1.29 μg $mL^{-1}$), compared with amphotericin B ($IC_{50}$ = 0.04 μg $mL^{-1}$). These findings highlight the chemical diversity and pharmacological relevance of Amaryllidaceae species.

**Keywords:** GNPS, mass spectrometry, FBMN, antiparasitic activity, *Ismene amancaes*

## Introduction

The continuous development of analytical and computational approaches has significantly driven research on plant-derived natural products. The evolution of analytical techniques, particularly mass spectrometry-based approaches, has enabled a precise and comprehensive analysis of the complex metabolic profiles present in plant extracts.[1,2] As the analytical techniques improve, the primary challenge shifts to efficiently interpreting and organizing the massive datasets generated. In this context, bioinformatics and chemoinformatics provide computational tools for data processing allowing a deeper understanding of the chemical complexity of living organisms.[1-3]

The Global Natural Products Social Molecular Networking (GNPS) is an open-access platform designed to facilitate the organization, sharing, and annotation of mass spectrometry data through community-driven

*e-mail: warley.borges@ufes.br; wandersonromao@gmail.com
Editor handled this article: Hector Henrique F. Koolen (Associate)
This publication is part of the special issue "Omics Sciences"

analysis.[4-6] One of its main analytical resources is molecular networking, a computational approach that connects molecules based on similarities in their fragmentation patterns, enabling the visualization of structural relationships among compounds.[7-9] This strategy has been widely applied in natural products research, including studies based on liquid chromatography-mass spectrometry (LC-MS) low-resolution data, as it supports comparative spectral analysis and aids in the annotation of complex mixtures. In plant metabolomics, the use of GNPS-based molecular networking has contributed to simplifying compound identification, expanding the exploration of chemical diversity, and supporting the investigation of biologically relevant metabolites.[8-10]

The Amaryllidaceae plants are a well-known source of an exclusive group of isoquinoline-like alkaloids that have attracted significant interest due to their biological properties and therapeutic potential.[5] This family comprises more than 70 genera and subgenera and approximately 800 species distributed across tropical and subtropical regions worldwide. In Brazil, around 19 genera and 157 species are distributed throughout the Southeast, Central-East, South, North, and Northeast regions. Species of the Amaryllidaceae family have been used therapeutically mainly due to their antineoplastic, antioxidant, antiviral, and antimicrobial activities.[5] Although Amaryllidaceae alkaloids have been associated with several biological activities, their potential against *Leishmania* species remains insufficiently explored. Given the clinical relevance of leishmaniasis and the ongoing demand for new therapeutic alternatives, this gap further supports the purpose of the present study. Methanolic extracts from 52 wild and commercial Amaryllidaceae species collected from different regions of Brazil and other Latin American countries were analyzed by low-resolution LC-MS, and alkaloid annotation was performed through feature-based molecular networking (FBMN). In addition, the extracts were evaluated for their antileishmanial activity to investigate possible relationships between alkaloid profiles and therapeutic potential against the parasite.

## Experimental

### General experimental procedures

For extraction procedures, analytical-grade methanol was obtained from Synth (Diadema-SP, Brazil). High-performance liquid chromatography (HPLC) grade methanol (Sigma-Aldrich, USA) was used for sample dilution and preparation of reference compounds. Formic acid (0.1% v/v) was used to acidify both Milli-Q water and methanol, constituting mobile phases A and B for chromatographic analyses. All samples and solutions were filtered using 0.22 µm polytetrafluoroethylene (PTFE) syringe filters (Allcrom, São Paulo, Brazil).

Antileishmanial assays were performed using *Leishmania* (*Leishmania*) *amazonensis*, strain PH8 (IFLA/BR/67/PH8). Parasites were cultured in the medium of Schneider or RPMI 1640 (Sigma-Aldrich, USA), supplemented with fetal bovine serum (20% v/v, Cultilab, Brazil), penicillin (10 IU $mL^{-1}$), and streptomycin (100 µg $mL^{-1}$). Cell viability and cytotoxicity were assessed using a resazurin solution (0.2 mg $mL^{-1}$, Sigma-Aldrich), following the AlamarBlue® protocol (Bio-Rad, 2020). Cytotoxicity assays were conducted using the murine fibroblast cell line NIH/3T3 (ATCC CRL-1658).

A panel of nineteen Amaryllidaceae alkaloids previously isolated[11-15] was used to construct a reference sequential tandem mass spectrometry (MS/MS) spectral library.

Methanolic extracts were concentrated under reduced pressure using a rotary evaporator (model R-3, BUCHI) coupled to a V-100 vacuum pump (BUCHI, Valinhos, Brazil) and a thermostatic water bath (SolidSteel, Piracicaba, Brazil). Chromatographic and mass spectrometric analyses were carried out using a Vanquish UHPLC system coupled to an LTQ XL™ linear ion trap mass spectrometer (Thermo Scientific, Germany) equipped with an electrospray ionization (ESI) source operating in positive ion mode. An Accucore C18 column (Thermo Scientific) was employed for chromatographic separations. Absorbance measurements in the resazurin-based assays were recorded using a Varioskan LUX Multimode Microplate Reader (Thermo Scientific). Mass spectrometric data acquisition was performed using Xcalibur software (version 2.2; Thermo Fisher Scientific). LC-MS data processing was conducted in MZmine (version 3.9.0, mzio GmbH, Bremen, Germany, 2023), and molecular networking analyses were performed on the GNPS platform (Center for computational mass spectrometry, California, 2016), with data uploaded via WinSCP (version 5.21.8, WinSCP, 2023). Molecular networks were visualized using Cytoscape (version 3.10.1, Cytoscape Consortium, NRNB, USA, 2024). Half-maximal inhibitory concentration ($IC_{50}$) and half-minimum cytotoxic concentration ($CC_{50}$) values were calculated by linear regression using GraphPad Prism (version 5, GraphPad software, Boston, MA, 2008). MS/MS dereplication and spectral annotation were carried out using the DEREPLICATOR tool implemented within the GNPS platform as previously described.

### Plant material and extraction

Bulbs from wild species were obtained and properly documented from locations across

Brazil (Espírito Santo, Goiás) and Latin America (Peru). In Brazil, bulbs of *Habranthus robustus* and *Hippeastrum reticulatum* were kindly provided, in cultivation, by Prof Dr Warley de Souza Borges (Domingos Martins-ES), while *Hippeastrum puniceum* was collected in a garden in Vitória-ES (voucher specimen VIES 48418). *Crinum scabrum* were collected at Goiandira-GO, Brazil (voucher specimen VIES 24824). Bulbs of cultivated plants of *Sprekelia formosissima*, *Eucharis amazonica*, and *Zephyranthes citrina* were acquired through online commercial suppliers. From Latin America, dried and ground bulbs of *Ismene amancaes* were kindly provided by Prof Marilú Roxana Soto-Vásquez (Facultad de Farmacia y Bioquímica, Universidad Nacional de Trujillo, Peru) with voucher specimen 63331 HUT. Commercial bulbs of *Hippeastrum* hybrids (marketed as "*Amaryllis*") were purchased from Toca do Verde (Tietê-SP, Brazil). A complete list of all 52 analyzed species can be found in Table S1 (Supplementary Information (SI) section). Access to genetic heritage was registered in the Brazilian National System for the Management of Genetic Heritage and Associated Traditional Knowledge (SisGen) under code A012E5E.

Fresh plant material was processed to separate bulbs from the species, which was then dried in an oven (Ethik Technology, São Paulo, SP, Brazil) at a controlled temperature of 45-55 °C for seven days. The data regarding dry mass, crude extract mass obtained, and the calculated extraction yield are provided in Table S2 (SI section). After this process, the dried material was ground, weighed, and properly documented.

Subsequently, the ground material was exhaustively macerated to obtain the methanolic crude extract. As mentioned, 5 mL of analytical-grade methanol (Synth, Diadema, SP, Brazil) *per* gram of dried material were added in each maceration cycle during the grinding process. The ground material was macerated for 48 h and repeated twice. After filtration, the solvent was combined and removed with a rotary evaporator under reduced pressure (model R-3, V-100 vacuum pump, BUCHI, Valinhos, Brazil and a SolidSteel thermostatic bath, Piracicaba, Brazil) to obtain the final crude methanolic extract.

### LC-MS analysis

The methanolic extracts from commercial and wild Amaryllidaceae species were dissolved in HPLC-grade methanol (Sigma-Aldrich, USA) at a concentration of 1.0 mg $mL^{-1}$ and filtered using 0.22 µm PTFE syringe filters (Allcrom, São Paulo, Brazil). Subsequently, 0.5 mL of the stock solution was diluted to 1.0 mL before injection into the instrument. A total of nineteen compounds of different chemical skeletons (haemanthidine, galanthamine, crinamine, pseudolycorine, albomaculine, lycorine, tazettine, crinine, ismine, 2-*O*-methylcandimine, galanthine, 3-epimacronine, 8-*O*-desmethylhomolycorine, *O*-methyllicorenine, 2-α-7-dimethoxyhomolycorine *N*-oxide, 2-α-methoxyhomolycorine, pretazettine, candimine, and hippeastrine). Each compound was prepared at a concentration of 1.0 mg $mL^{-1}$ in methanol and filtered using 0.22 µm PTFE syringe filters (Allcrom, São Paulo, Brazil). Then, 10 µL of the stock solution were diluted to 1.0 mL with HPLC-grade MeOH for analysis. Individual analyses were performed for each compound, and a pooled quality control (QC) sample containing all compounds was also prepared and analyzed under the same conditions.

### Analysis parameters

Liquid chromatography separations were performed using an Accucore C18 column (150 × 4.6 mm, 2.6 µm; Thermo Scientific). The injection volume was 5 µL, and the mobile phase flow rate was set at 0.5 mL $min^{-1}$. A gradient elution method was employed using water acidified with 0.1% (v/v) formic acid (solvent A) and methanol acidified with 0.1% (v/v) formic acid (solvent B). The gradient started at 10% B, increased to 80% B over 25 min, held for 2 min, and then returned to the initial conditions at 28 min, which were maintained until the end of the chromatographic run at 30 min. The column temperature was maintained at 35 °C.

Mass spectra were acquired in the *m/z* range of 50-1000 using data-dependent acquisition (DDA) mode with centroid detection, and the top three most intense precursor ions were selected for fragmentation. The ESI source parameters were as follows: source voltage, 4 kV; source temperature, 380 °C; sheath gas flow rate, 35 (arbitrary units); auxiliary gas flow rate, 10 (arbitrary units); capillary voltage, 49 V; capillary inlet temperature, 350 °C; and tube lens voltage, 80 V MS/MS fragmentation was performed using collision-induced dissociation (CID) with 35% normalized collision energy. Data acquisition was carried out using Xcalibur software (version 2.2; Thermo Fisher Scientific).

Mass spectra were acquired in positive ion mode due to its higher sensitivity for alkaloid analysis, as these compounds contain basic nitrogen atoms that readily protonate, generating intense $[M + H]^+$ ions. Fragmentation patterns were further evaluated to provide complementary structural information for compound identification.

### Feature-based molecular networking

LC-MS files in ".raw" format were imported directly into MZmine for data processing. Mass detection was first applied with noise thresholds of $1.5 \times 10^4$ for $MS^1$ and $1.0 \times 10^3$ for $MS^2$. Chromatograms were generated using the Automated Data Analysis Pipeline (ADAP) algorithm with a minimum of 4 scans, intensity threshold of $1.0 \times 10^3$, peak height of $3.0 \times 10^3$, and an *m/z* tolerance of 0.5 Da. Peaks were resolved with the local minimum feature resolver, applying an $t_R$ tolerance of 0.30 min and an *m/z* tolerance of 0.05 Da for $MS^2$ pairing. Isotopes were grouped with an *m/z* tolerance of 0.5 Da, $t_R$ tolerance of 0.05 min, and maximum charge of 3. Feature alignment was performed with the join aligner (*m/z* tolerance 0.5 Da, $t_R$ tolerance 0.30 min). The feature list was then filtered to retain only peaks with MS/MS scans, followed by blank subtraction. Gap filling was applied with an intensity tolerance of 10%, *m/z* tolerance of 0.5 Da, and $t_R$ tolerance of 0.1 min. Data were normalized by average peak height. Feature grouping was conducted using correlation grouping ($t_R$ tolerance 0.055 min, minimum peak height $1.0 \times 10^3$, correlation intensity threshold $5.0 \times 10^2$). The aligned feature list was exported in ".mgf" and ".csv" formats for molecular networking in GNPS, together with the metadata file.[16]

MS/MS spectra from isolated Amaryllidaceae alkaloids were converted from ".raw" to ".mzML" and uploaded to the GNPS platform to expand the spectral library, where user-contributed data are classified as bronze-quality reference spectra. Feature-based molecular networking was performed by uploading the ".csv", ".mgf", and metadata files generated in MZmine. The data were filtered to remove precursor-related ions and reduce spectral noise, retaining only the most intense fragment ions. The precursor and fragment mass tolerances were set to 2 Da and 0.2 Da, respectively.

A molecular network was constructed by retaining edges with a cosine score above 0.7 and at least four matching peaks. Furthermore, edges between two nodes were kept in the network only if each node was among the four most similar nodes. The maximum molecular family size was restricted to 10, and lower-scoring edges were removed until the family size met this threshold. Spectra in the network were then searched against the GNPS spectral libraries using the same filtering criteria, and library matches were accepted only when the score was above 0.6 with at least four matching peaks.

For MS/MS spectrum annotation, DEREPLICATOR was employed as described by Mohimani *et al.*[17] The molecular networks were visualized using Cytoscape, following the methodology described by Shannon *et al.*[18]

### Antileishmanial activity

#### Anti-promastigote assays against *L. amazonensis*

Promastigote forms ($2 \times 10^5$) of *L. amazonensis*, strain PH8 (IFLA/19BR/67/PH8), at the logarithmic growth phase in properly supplemented in the medium of Schneider, were distributed into 96-well plates containing the extracts at different concentrations, ranging from 1000 to 15125 μg $mL^{-1}$ The plates were incubated for 48 h at 26 °C. After each incubation period, 5 μL of resazurin solution at 0.2 mg $mL^{-1}$ (Sigma-Aldrich, USA) were added to each well. After an additional 4 h of incubation at 26 °C, absorbance readings were taken at 570 and 600 nm using a SpectraMax Microplate reader (Tmolecular Devices, USA). For resazurin, the viability calculation for all wells was carried out based on the formula and instructions provided by the manufacturer AlamarBlue® (BioRad, 2020), as follows:

$$\%\ \text{viability difference} = \frac{(O2 \times A1) - (O1 \times A2)}{(O2 \times P1) - (O1 \times P2)} \times 100 \quad (1)$$

where O1 is the molar extinction coefficient (ε) of oxidized resazurin at 570 nm, O2 is the ε of oxidized resazurin at 600 nm, A1 is the absorbance of the test well at 570 nm, A2 is the absorbance of the test well at 600 nm, P1 is the absorbance of the untreated control well at 570 nm, and P2 is the absorbance of the untreated control well at 600 nm. The average reading of the control wells containing only culture medium was considered as 100% viability, and the percentage of viability for the treated samples was calculated based on the control readings. The inhibitory concentration ($IC_{50}$) was calculated by linear regression, plotting the log10 of each inhibitor concentration against the percentage activity using Prism 5 software.

#### Cytotoxicity assay

NIH/3T3 cells (ATCC CRL-1658, mouse fibroblast cell line) were cultured in 96-well plates ($1.1 \times 10^5$ cells *per* well) in properly supplemented RPMI 1640 medium. Cells were allowed to adhere overnight at 37 °C in 5% $CO_2$. The medium was then replaced with fresh RPMI containing compound concentrations ranging from 1000 to 15125 μg $mL^{-1}$, and the plates were incubated under the same conditions for 48 h. Fibroblasts cultured with medium alone were used as the viability control.

Next, 5 μL of resazurin solution at 0.2 mg $mL^{-1}$ (Sigma-Aldrich, USA) were added to each well, and plates were incubated for 4 h at 37 °C in 5% $CO_2$. Absorbance was measured at 570 and 600 nm using a SpectraMax Microplate Reader (Molecular Devices, USA). Cell

viability for all wells was calculated based on the formula and instructions provided by the AlamarBlue® manufacturer (BioRad, 2020). Cell viability was assessed from optical density and compared to untreated cells.

The cytotoxic concentration ($CC_{50}$) was calculated by non-linear regression, plotting the $\log_{10}$ of each inhibitor concentration against the percentage activity using Prism 5 software. The selectivity index (SI) was obtained by calculating the ratio between $CC_{50}$ and $IC_{50}$ for each extract.

## Results and Discussion

### Feature-based molecular networking (FBMN)

The structuring of the clusters, or groups, considered multiple factors and was subsequently refined using Cytoscape software to improve data interpretation. These factors included edge strength (stronger connections representing higher similarity between nodes, cosine score ranging from 0.7 to 1.0), node coloring, indicating sample origin, and node labels which reflect the precursor ion $[M + H]^+$. Annotations for each node were based on spectral library matches from GNPS (Figure S1, SI section), while identifications were confirmed by comparison with the respective standards. Each compound was individually verified and compared with literature data on the identification of Amaryllidaceae alkaloids in LC-MS experiments.

It is important to emphasize that in metabolomics investigations, a clear distinction must be made between "annotation," which corresponds to confidence levels 2 to 4, and "identification," which corresponds to confidence level 1.[19,20] These confidence levels, as defined by Sumner *et al.*,[19] range from unknown to precise metabolite identification. According to Sumner *et al.*,[19] this scale ranges from level 1 (highest confidence) to level 4 (lowest confidence). Currently, at the database-search stage, compound name associations usually carry low confidence. Therefore, comparison with MS/MS libraries can raise it to level 2, while level 1 requires both MS/MS spectral matching and retention time matching with authentic standards.[20]

With this framework, cluster analysis was initially focused on all nodes grouped with nodes of authentic standards, followed by those with precursor ions *m/z* correlating to characterized substances for annotation.

FBMN analysis showed those substances clustered according to the Amaryllidaceae alkaloid skeleton type, with the exception of the alkaloid galanthamine. A total of six molecular families were assigned to these structures, with five different skeleton types detected: homolycorine-type, haemanthamine-type, pretazettine-type, lycorine-type, and galanthamine-type, as illustrated in Figure 1.

### Galanthamine- and lycorine-type clusters

Galanthamine- and lycorine-type alkaloids, belonging to the Amaryllidaceae family, are notable for their complex chemical structures and remarkable biological properties.[21-29] These bioactive compounds have attracted considerable attention due to their potential therapeutic applications, with galanthamine, in particular, being used for the palliative management of mild to moderate Alzheimer's disease.[30-32] The biological significance of the galanthamine-type skeleton has prompted the development of liquid chromatography methodologies

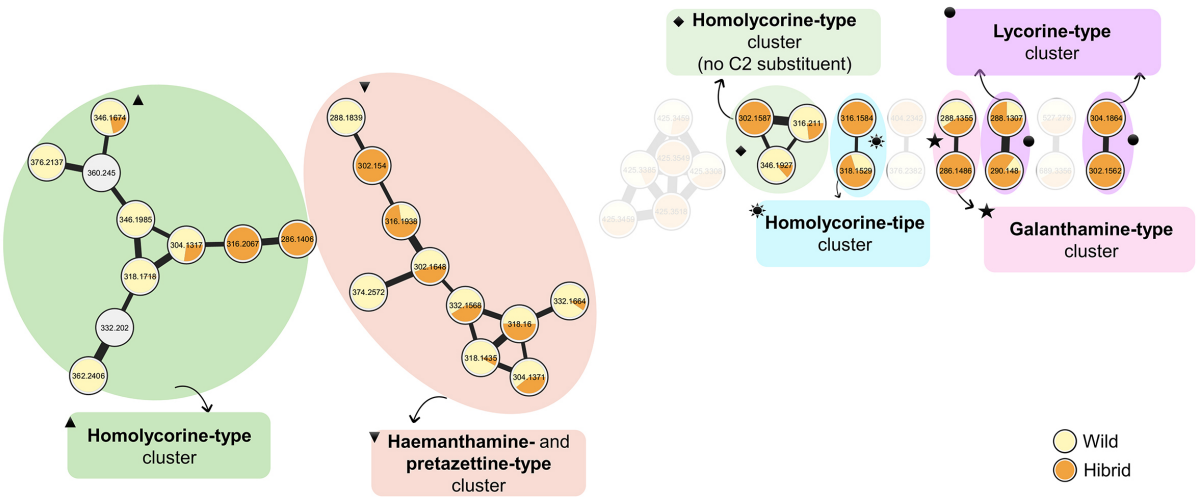


**Figure 1.** Highlight of the families observed for each type of Amaryllidaceae alkaloid skeleton. Five types were identified: homolycorine (green), haemanthamine (orange), pretazettine (orange), galanthamine (pink), and lycorine (purple).

for detection/quantification of Amaryllidaceae alkaloids in plant extracts or biological fluids.[33-41] Molecular networking, by enabling the visualization of multiple analyses, significantly contributes to the understanding of the chemical complexities associated with these alkaloids across different matrices or species.

Figure 2 provides an enlarged view of clusters formed by nodes corresponding to galanthamine- and lycorine-type alkaloids. The structures shown in Figure 2 indicate a match with the injected standards, which are represented by the gray color in the nodes. The remaining features were manually annotated through spectral comparison with the literature. Table 1 presents the retention time information, as well as the fragments obtained for each annotated and identified compound.

The galanthamine-type skeleton, composed of 15 carbon atoms, results from a para-ortho oxidative coupling of the phenol group of 4'-*O*-methyl-norbelladine (Figure S2, SI section).[33] To date, 47 alkaloids have been reported within this specific subgroup.[40] Its structural diversity arises from the variety of substituents present at C2, C3, C9, C11, and on the nitrogen atom, resulting in two distinct subtypes: galanthamine, which features a double bond at C4-C4a, and lycoramine, which lacks the double bond at C4-C4a.[42,43] The substituents on the nitrogen include methyl and acetyl groups, as well as hydrogen and oxygen (as *N*-oxide), among others.[5]

Galanthamine is one of the most studied alkaloids in the Amaryllidaceae family because it is used as a commercial drug to treat Alzheimer's disease. For this alkaloid, observed in the cluster with a precursor ion at *m/z* 288 and a retention time ($t_R$) of 4.95 min, the fragment ion at *m/z* 270 is formed by the neutral loss of $H_2O$. Each annotation was carefully checked by comparing the experimental spectral data with data from the reference library, as illustrated in Figures S1 and S4 (SI section).

Next to the galanthamine node, there is an $[M + H]^+$ ion at *m/z* 286 that the NIST14 library misidentified as glicitine (Figure S5, SI section). The connection between these nodes represents a spectral similarity, with a cosine score greater than 0.7, suggesting a structure close to galanthamine. Consequently, a literature search was

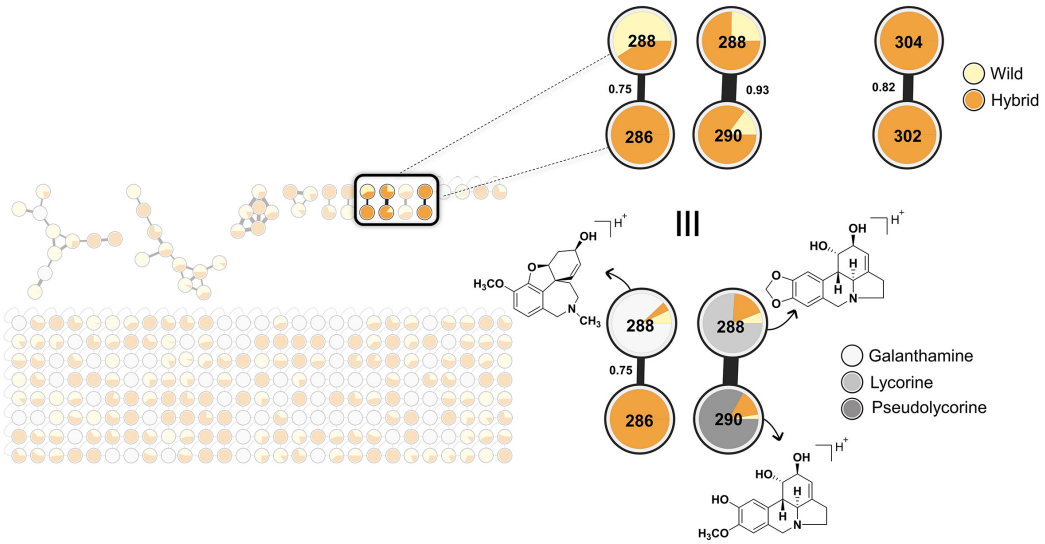


**Figure 2.** Enlarged view of the clusters formed by nodes corresponding to galanthamine- and lycorine-type alkaloids. Nodes filled in gray represent the analyzed standards, while yellow and orange indicate wild and hybrid species, respectively. The remaining nodes were manually annotated through spectral comparison with the literature and are listed in the Table 1.

**Table 1.** Annotation, retention times, and fragments identified for the lycorine- and galanthamine-type alkaloid clusters

| No. | Annotation | $t_R$ / min | $[M + H]^+$ | MS/MS |
|---|---|---|---|---|
| **1** | 2-*O*-Methylpseudolycorine | 2.81 | 304 | 286, 268, 179, 147, 126 |
| **2** | Pseudolycorine | 2.89 | 290 | 272, 254, 244, 222, 179, 147, 124 |
| **3** | Lycorine | 4.13 | 288 | 270, 252, 222, 177, 147 |
| **4** | Hipamine | 3.77 | 302 | 284, 177, 147, 126 |
| **5** | Galanthamine | 4.96 | 288 | 270, 231, 225, 213, 198 |
| **6** | Narwedine | 7.23 | 286 | 269, 255, 242, 237, 229, 225 |

$t_R$: retention time; MS/MS: sequential tandem mass spectrometry.

conducted to investigate studies that employed LC-MS techniques for the comparison of fragments at *m/z* 269, 255, 242, 237, 229, and 225. Tian *et al*.[44] identified narwedine as the $[M + H]^+$ ion corresponding to *m/z* 286, associating the fragment ion at *m/z* 255 with a neutral loss of $CH_3NH_2$.[44] Additionally, the researchers observed another prominent fragment ion at *m/z* 229, possibly generated by the loss of a $C_3H_7N$ unit (58 Da). Therefore, in this molecular network, the ion at *m/z* 286 connected to galanthamine was assigned to the alkaloid narwedine.[44]

Another $[M + H]^+$ ion at *m/z* 288, shown in Figure S6 (SI section), presented the most intense fragment ions at *m/z* 270, 252, and 222, resulting from the successive losses of $H_2O$ (18 Da), $2H_2O$ (36 Da), and $CH_2O$ (30 Da), respectively, as proposed in Figure S6 (SI section). Additionally, fragments at *m/z* 177 $[M + H - C_6H_9NO]^+$ and 147 $[M + H - C_7H_{11}NO_2]^+$ were also observed at lower intensities; both are characteristic of the Retro Diels-Alder (RDA) cleavage in the alkaloid lycorine.[44]

Lycorine-type alkaloids show exceptional structural diversity, with 119 compounds reported so far,[5] a pattern consistent with findings from other Amaryllidaceae species, such as *Worsleya procera*, which also exhibits a broad spectrum of structurally diverse alkaloids. The structural complexity of these alkaloids arises from the variability of substituents on nearly every carbon atom of the core skeleton, as well as on the nitrogen atom, the configuration of specific substituents, and the degree of aromatization in certain rings. Therefore, the precursor ion at *m/z* 290, clustered with the lycorine node and showing a cosine score above 0.9, indicates a highly similar structure. In this case, the spectral library successfully identified it as the alkaloid pseudolycorine, and the molecular network confirmed that this same node corresponds to the injected pseudolycorine standard. Once again, the predominant fragment ions result from the successive losses of $H_2O$, $2H_2O$, and $CH_2O$, giving rise to fragment ions at *m/z* 272, 254, and 222, respectively, as also observed for lycorine. The key structural feature distinguishing this alkaloid is the absence of the methylenedioxy group found in lycorine, replaced by a methoxy group at position 8 and a hydroxyl group at position 9. Due to these substitutions, the characteristic RDA cleavage fragment ion appears at *m/z* 179, as shown in Figure S7 (SI section).

The third cluster presented two connected $[M + H]^+$ ions with a mass difference of 2 Da between them. Spectral analysis using the GNPS libraries did not reveal any matches; therefore, a manual inspection of the fragment ions observed at *m/z* 304 and 302 was conducted. In general, a cosine score above 0.8 indicates high spectral similarity between the two compounds, and the 2 Da difference between the nodes suggests the substitution of the methylenedioxy group at positions C8 and C9 by methoxy and hydroxyl groups, respectively. Both ions exhibited water loss (18 Da) as the base peak and showed other fragment ions resulting from RDA cleavage, as illustrated in Figure S8 (SI section). Based on the fragment analysis, the structures were annotated as 2-*O*-methylpseudolycorine (*m/z* 304) and hipamine (*m/z* 302).

Considering the rationalized annotations made for lycorine-type skeleton, it is evident that the substituents on ring C may be responsible for the clustering of these nodes, i.e., compounds with identical substitution on ring C are grouped into a family regardless C8 and C9 substitution pattern.

### Pretazettine- and haemanthamine-type clusters

Haemanthamine- and pretazettine-type alkaloids share a 15-carbon skeleton and are products of a *para–para*' oxidative phenolic coupling in 4'-*O*-methyl-norbelladine (Figure S9, SI section).[29] According to Berkov *et al*.,[5] 76 haemanthamine-type compounds and 32 pretazettine-type compounds are known. The structural variation of these alkaloids results from the presence of a wide range of substituents at various positions of the carbon skeleton, together with variation in the degree of aromatization of ring C. Notably, haemanthamine-type alkaloids with a substituent at C6 (hydroxyl, methoxyl, or ethoxyl) are typically observed as a mixture of epimers in solution.[5,42]

Noteworthy, some compounds isolated or detected in natural samples may be artifacts formed after the acid-base isolation process. For example, tazettine is an artifact of pretazettine isolation, formed under basic conditions as a result of an intermolecular rearrangement.[5,45] Hence, the evaluation of crude Amaryllidaceae extract avoiding any acid-base procedure becomes particularly relevant.

The cluster identified for these types of structures revealed three matches with GNPS standards and libraries, including one duplicated match, indicating the likely presence of epimers. Additionally, four annotations were performed manually by comparing the experimental fragmentations with the literature, as reported in Table 2 and Figure S10 (SI section). These analyses also enabled the determination of the identity of each epimer.

Two of the features annotated by the library and matching the standards corresponded to the precursor ions $[M + H]^+$ at *m/z* 302 ($t_R$ = 8.90 min) and 332 ($t_R$ = 8.50 min) at the center of the cluster in Figure S10 (SI section). After verifying the spectral similarity, it can be assumed that these ions are related to the alkaloids crinamidine and pretazettine, respectively. Although they represent

**Table 2.** Annotation, retention times, and fragments found for the clusters of haemanthamine- and pretazettine-type alkaloids

| No. | Annotation | $t_R$ / min | $[M + H]^+$ | MS/MS |
|---|---|---|---|---|
| **7** | *N*-Oxide 11-hydroxyvitatine | 4.36 | 304 | 286, 268, 227, 211 |
| **8** | Hamaine / bulbispermine | 7.05 | 288 | 270, 252, 244, 229, 211 |
| **9** | 11-*O*-Methylcrinamine | 8.03 | 316 | 284, 273, 266, 256, 240, 227, 213, 211, 181 |
| **10** | Crinamine | 8.90 | 302 | 284, 270, 259, 252, 226, 211, 181 |
| **11** | Pretazetine | 8.50 | 332 | |
| **12** | *epi*-Haemanthidine | 8.91 | 318 | 300, 286, 268, 259, 241, 227, 211, 199 |
| **13** | 6-Methylhaemanthidine | 9.13 | 332 | 259, 227 |
| **14** | Haemanthidine | 9.72 | 318 | 300, 286, 268, 259, 241, 227, 211, 199 |
| **15** | 3-*O*-Desmethyl-3-*O*-(3'-hydroxybutanoyl)haemanthamine | 10.82 | 374 | 330, 270, 252, 226, 211, 181 |

$t_R$: retention time; MS/MS: sequential tandem mass spectrometry.

different skeleton types, both arise from a *para–para*' type coupling, which justifies the connection between these two features in the molecular network. It is worth noting that the molecular network generated by GNPS was able to distinguish pretazettine from another ion of the same mass (*m/z* 332) based on their fragmentation spectra, since one of them showed a spectral match with the library and the other did not.

The alkaloid pretazettine ($[M + H]^+$, *m/z* 332) was connected to two ions of 318 Da, both identified as the alkaloid haemanthidine by the GNPS spectral library. This duplicated identification occurred due to the spectral similarity of both precursor ions $[M + H]^+$, at *m/z* 318, with the haemanthidine spectrum deposited in the library, as indicated by the cosine score of 0.89 shown on the edge between them. Due to these factors, one of the ions can be assigned as the epimer of haemanthidine, named *epi*-haemanthidine. The occurrence of this epimer is considered common, since these alkaloids are frequently found as epimeric mixtures.[10] According to Berkov *et al.*,[10] these epimeric forms have been suggested to be interchangeable, that is, they may coexist in equilibrium and can be easily interconverted under certain conditions.[43] Additionally, it is well-known that the conversion of haemanthamine into haemanthidine/*epi*-haemanthidine and subsequently into pretazettine occurs in an essentially irreversible manner, a process illustrated in Figure S11 (SI section).[46]

The correct assignment of the identification between haemanthidine and *epi*-haemanthidine for each precursor ion was made possible by integrating the standards into the analysis. It was observed that the standard corresponding to haemanthidine showed predominant filling in the node at *m/z* 318, illustrated in light gray in Figure S11 (SI section). In addition, a literature search was conducted regarding the fragmentation data observed for these compounds. According to a study by Torras-Claveria *et al.*,[47] which employed the ESI(+)MS/MS technique to analyze various Amaryllidaceae alkaloids, the base ion of the alkaloid haemanthidine was identified as the fragment ion at *m/z* 227, whereas the fragment ion at *m/z* 286 showed an intensity of 40%.[47] Based on this, the node at *m/z* 318 ($t_R$ = 9.72 min) was assigned to haemanthidine, since its spectrum presented the base ion 227, as illustrated in Figure S12 (SI section), whereas the node represented by *m/z* 318 ($t_R$ = 8.91 min) presented *m/z* 286 as the base ion. Therefore, the latter was assigned to alkaloid *epi*-haemanthidine.

In this cluster, a feature at *m/z* 304 was observed connected to the alkaloids haemanthidine and *epi*-haemanthidine, indicating a structure belonging to the haemanthamine core. The fragment ions *m/z* 286 and 268, the base ion at *m/z* 227, and the ion at *m/z* 211 were detected. The first two ions indicate two consecutive $H_2O$ losses (18 Da). The base ion at *m/z* 227 results from the loss of 41 Da from *m/z* 268, suggesting the elimination of the amine ethano brigde moiety. A literature search revealed the same fragments reported for the 11-hydroxyvittatine *N*-oxide.[36]

In addition, a node corresponding to *m/z* 332 was observed, connected solely to the feature at *m/z* 318.16 previously assigned to *epi*-haemanthidine. The cosine score of 0.81 indicates high similarity between these two compounds. The 14 Da difference between these ions suggests the substitution of a hydroxyl group by a methoxyl group at position C-6 or C-11 of *epi*-haemanthidine. Due to the prominent fragment ions at *m/z* 259 and 227, this node is suggested to correspond to the alkaloid 6-methylhaemanthidine.

Two other features are connected to the node corresponding to crinamidine. The node represented by *m/z* 316 ($t_R$ = 8.03 min), showed a cosine score greater than 0.9, indicating high similarity with crinamidine. A noteworthy observation was the absence of the fragment ion at *m/z* 270 and the formation of the ion at *m/z* 284. After

consulting the literature,[48] this compound was identified as 11-*O*-methylcrinamidine (Figure S13).

The other node, represented by *m/z* 374 and found at a retention time of 10.8 min, exhibited a relatively high cosine score, also indicating a structural similarity to crinamidine. The fragmentation pattern observed for this compound showed fragment ions at *m/z* 270, 213, and 211, as in crinamidine. However, a loss of 44 Da from the molecular ion was observed, as evidenced by the presence of the fragment ion at *m/z* 330. After an extensive literature search for studies employing LC-MS, no match was found for this *m/z* 374 ion. From the 75 haemanthamine-type structures summarized by Berkov *et al*.,[10] only two alkaloids named 6β-acetoxycrinamidine and 3-*O*-desmethyl-3-*O*-(3'-hydroxybutanoyl)haemanthamine had a similar fragmentation pattern and molecular ion as those observed for crinamidine. It is observed that the base ion generated is at *m/z* 270, as in crinamidine, along with other fragment ions also related to the crinamidine skeleton, such as *m/z* 181, 211, 226, 242, and 252. Based on these data, this node was assigned to the alkaloid 3-*O*-desmethyl-3-*O*-(3'-hydroxybutanoyl)haemanthamine, since the loss of 104 Da corresponds to the *O*-(3'-hydroxybutanoyl) moiety highlighted in red in Figure S14 (SI section).

The *m/z* 302 ion connected to 11-*O*-methylcrinamidine, as well as the *m/z* 288 ion, showed no spectral match in the library. Despite an extensive literature search, it was not possible to identify these compounds. However, due to the presence of diagnostic fragment ions such as *m/z* 270, 229, and 211 for the precursor ion at *m/z* 288, and *m/z* 286, 229, and 211 for the precursor ion at *m/z* 302, in addition to their connectivity with a haemanthamine-type alkaloid, it is suggested that these compounds likely possess a structure similar to that of haemanthamine.

### Homolicorine-type clusters

Alkaloids with a 15-carbon homolycorine-type skeleton are formed by a rearrangement of the lycorine-type skeleton via the conversion of norpluviine into lycorenine (Figure S15, SI section). To our knowledge, 80 natural compounds of this group are known. The homolycorine-type alkaloids can be divided into two main series, based on the saturation of the C3-C4 bond. The known derivatives of this group, including homolycorine, possess a C3-C4 double bond and exhibit a *cis*-B/C ring junction, with protons at C1 and C10b in *S*-configuration.[43]

In this molecular networking study, the formation of three clusters related to this type of Amaryllidaceae alkaloid structure was observed, as illustrated in Figure S16 (SI section). The first and largest cluster contained ten homolycorine derivatives, with five of them identified by the GNPS library, but one assigned as lycorine-type (explanation below). Two alkaloids identified in this group correspond to the standards and were not found in the extracts of hybrid species nor in the extracts of wild species, as illustrated. The second cluster showed three nodes, with one of them having a spectral match. The same identification situation was found for the last cluster, which contained only two nodes related to each other. Information on retention time, precursor ion, and fragments is presented in Table 3.

The first cluster showed five matches with the GNPS spectral library, two of which were not present in any of the extracts. Two other alkaloids were manually annotated through comparison with the literature (Figure 3). It was observed that the majority of homolycorine derivatives were found in wild species.

Regarding the fragmentation data of homolycorine-type alkaloids, significant fragment ions were observed

**Table 3.** Annotation, retention times, and fragments found for the homolycorine-type alkaloid clusters

| No. | Annotation | $t_R$ / min | $[M + H]^+$ | MS/MS |
|---|---|---|---|---|
| **16** | Goleptine | 5.63 | 304 | 272, 254, 243, 227, 222,194 |
| **17** | Hippeastrine | 5.84 | 316 | 298, 280, 270, 267, 255, 239, 227, 191, 175, 126, |
| **18** | Candimine | 6.24 | 346 | 328, 310, 221, 125 |
| **19** | 8-*O*-Demethylhomolicorine | 6.87 | 302 | 300, 286, 268, 259, 241, 227, 211, 199 |
| **20** | Galanthine | 7.13 | 318 | 300, 286, 268, 257, 237, 215, 193, 162 |
| **21** | 2-O-Methylcandimine | 7.47 | 360 | 342, 331, 310, 292, 284, 252, 221, 140, 125, 110 |
| **22** | 2-α-Methoxyhomolicorine | 7.86 | 346 | 328, 314, 296, 278, 265, 255, 207, 140 |
| **23** | Dihydrohipeastrine / clivonine | 8.30 | 318 | 300, 282, 278, 265, 257, 239, 191 |
| **24** | 2-α-Dimethoxyhomolicorine | 8.38 | 376 | 344, 326, 237, 140 |
| **25** | Albomaculine | 8.98 | 346 | 328, 237, 110, 108 |
| **26** | *O*-Methyllicorenine | 10.86 | 332 | 314, 300, 282, 272, 257, 191 |
| **27** | 7-Methoxy-*O*-methyllicorenine | 13.24 | 362 | 344, 330, 302, 287, 221 |

$t_R$: retention time; MS/MS: sequential tandem mass spectrometry.

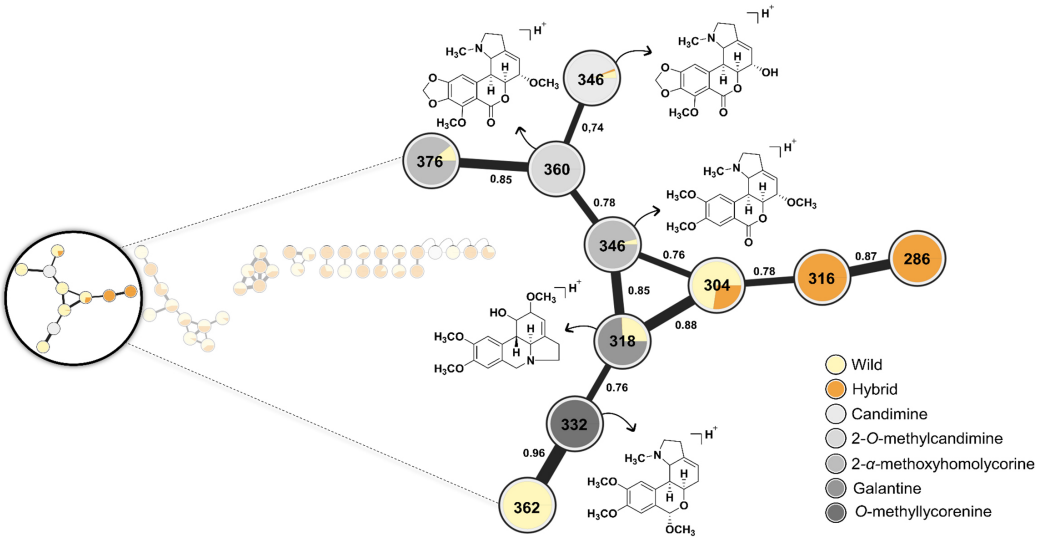


**Figure 3**. Visualization of the first cluster containing homolycorine-type alkaloids. Nodes filled in gray represent the analyzed standards, while yellow and orange correspond to wild and hybrid species, respectively. The remaining nodes were manually annotated.

due to RDA cleavage and the loss of some substituents (Figure S17, SI section). Few studies have identified homolycorine-type compounds by LC-MS, making the identification of the unannotated compounds more difficult.

The alkaloids candimine (*m/z* 346), 2-*O*-methylcandimine (*m/z* 360), galanthine *(m/z* 318), and *O*-methyllycorenine (*m/z* 332) were annotated by the spectral library and represented in the respective standard nodes. The compound represented by the $[M + H]^+$ ion at *m/z* 362 was designated as 7-methoxy-*O*-methyllycorenine due to its cosine score of 0.96 and the 30 Da difference between them, indicating high structural proximity to *O*-methyllycorenine. It was also possible to annotate the alkaloid goleptine (*m/z* 304) due to its close relationship with galanthine (*m/z* 318), with a cosine score of 0.9.

Interestingly, the alkaloids galanthine and goleptine are classified as having lycorine-type skeletons; however, the molecular network clustered them with the homolycorine alkaloids. Clustering in molecular networking can be sensitive to small structural variations, and the presence of specific features, such as functional groups, can lead to the formation of unexpected clusters. Therefore, even if the skeletons are initially classified as lycorine-type, other structural factors can lead to their association with homolycorine-type skeletons in the network analysis.

The ion at *m/z* 376, found predominantly in extracts from wild species, did not have a match in the library. However, a high spectral similarity was found with the compound 2-*O*-methylcandimine *(m/z* 360), as the cosine score between the two nodes is greater than 0.85. Furthermore, the molecular networking analysis demonstrates a high spectral similarity of this ion with the alkaloid 2-*O*-methoxyhomolycorine since the node for the *m/z* 376 ion shares the same color as the standard node for the latter. Based on this information and rationalizing the structural core of homolycorine alkaloids along with the experimental fragmentation pattern provided by GNPS, it was possible to tentatively propose a new structure. The fragmentation spectrum observed for this substance showed intense fragment ions at *m/z* 237 and 140, which originate from a RDA cleavage. The same ion at *m/z* 140 was found for 2-*O*-methylcandimine, suggesting the presence of a methoxy substituent at C2. However, it is noted that the ion at *m/z* 237 represents a 16 Da increase compared to the ion observed for 2-*O*-methylcandimine. This value indicates that, in addition to a methoxy group at C7, the methylenedioxy group is not present in this structure. Figure S18 (SI section) illustrates the proposed structure for this substance based on the fragmentation analysis.

The second cluster showed a connection among three nodes (Figure 4). The alkaloid albomaculine was annotated by the library, detected at a retention time of 9.51 min as an $[M + H]^+$ ion corresponding to *m/z* 346. Analysis of the connections and confirmation by the library indicate that albomaculine shares similar structural features and fragments with the other two compounds. The compound with an *m/z* of 302 was identified as the alkaloid 8-*O*-demethylhomolycorine, after comparing its fragmentation data with the literature and the standard.

It is noted that the substitution at C7 found in the alkaloid albomaculine leads to a drastic decrease in the cosine score of the edges connected to this *m/z* and 8-*O*-demethylhomolycorine remained above 0.9. Notably, this group had in common the double bond between C3-C4, a methoxy substitution at C9, and, consequently, the absence of the methylenedioxy group, but primarily

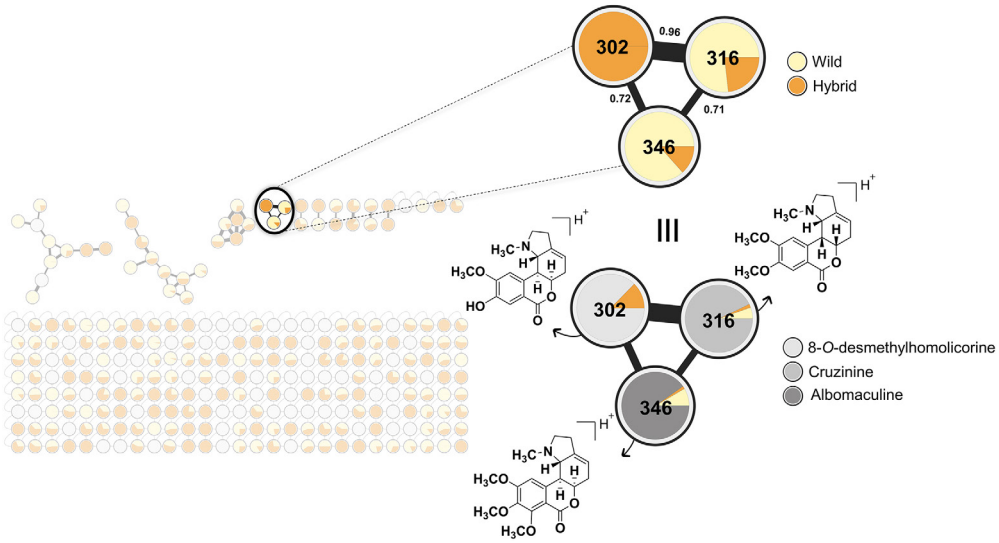


**Figure 4.** Expanded view of the clusters formed by nodes of homolycorine-type alkaloids. Nodes filled in gray represent the analyzed standards, while yellow and orange correspond to wild and hybrid species, respectively. The remaining nodes were manually annotated through spectral comparison with the literature, as presented in Table 3.

the absence of a substituent at C2. This last characteristic can be assigned to the ions observed at *m/z* 108 through an RDA mechanism. This same mechanism can lead to the formation of more intense ions, observed at *m/z* 237 for albomaculine and *m/z* 193 for 8-*O*-demethylhomolycorine, as demonstrated in Figure S19 (SI section). For all alkaloids identified in this cluster, the base peak was shown to be the loss of a water molecule (18 Da).

The third group is composed of only two nodes, as illustrated in Figure 5. This cluster, in fact, is a result of the delimitation set during the network construction procedure. As the molecular network was configured to display a maximum of ten connected compounds, these two members of the third group would most likely be connected to the first group, which had reached the established limit.

The node at *m/z* 316 was designated as hippeastrine due to its correspondence with the injected standard. For this alkaloid, fragment ions were observed from successive water losses at *m/z* 298 $[M + H - H_2O]^+$ and 280 $[M + H - 2H_2O]^+$, *m/z* 239, and from RDA fragments at *m/z* 191 and 126.[44] The node represented by *m/z* 318 was inconclusive due to a lack of information from the observed fragments in comparison with the literature. The 2 Da difference between the nodes suggests a possible substitution at the C8 and C9 positions with methoxy groups, as is also observed in the lycorine group. However,

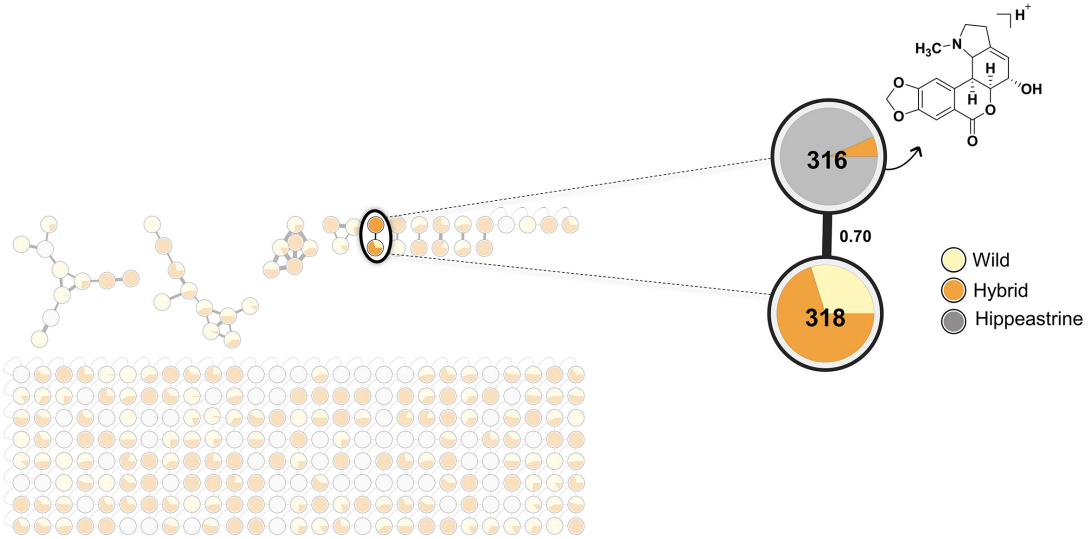


**Figure 5.** Expanded view of the clusters formed by nodes of alkaloids from the third homolycorine-type group. The node filled in gray represents the analyzed standard, while yellow and orange correspond to wild and hybrid species, respectively. Hippeastrine, *m/z* 316, was identified through the GNPS library and matched the injected standard node, whereas *m/z* 318 was manually annotated.

based on the observed ion at *m/z* 191, it is known that a methylenedioxy group is present, as in hippeastrine. The ions at *m/z* 300 and 282 were also assigned to successive water losses. Therefore, the mass difference can be attributed to the absence of the double bond between C3 and C4, corresponding to the alkaloids dihydrohippeastrine and clivonine, which differ only in the stereochemistry of the substituent at C2 (Figure S20, SI section).

### Unique nodes

The unique nodes are those not related to the families found in the molecular network. These can be generated by the delimitation of the cluster size and the minimum correspondence of fragment ions in the analysis parameters entered into GNPS, or by being a representative of a different nucleus. Additionally, the noise not fully filtered in the pre-processing within the mzMine3 software could have also played a role in this.

It was detected that most of the nodes present a mass of *m/z* 64 and 343 at retention times before 2 min and after 25 min, these retention times being related to the equilibration of the mobile phase in the chromatographic column. On the other hand, there are nodes with peculiar masses within the retention time related to the detection of the compounds. The delimitation of the molecular family size, and the required minimum number of fragments required led to presenting these nodes in an isolated manner. The molecular network was limited so that a cluster would exhibit a maximum of 10 nodes, with each node being able to be connected to four other nodes. In addition, another parameter for the analysis was the minimum of four fragments for the compatibility of the annotation.

As a result of this, the nodes related to the mobile phase were manually removed to facilitate the visualization of the nodes of greater relevance in this study. Among the 218 unique nodes found, 40% remained for a manual analysis of the fragmentation spectra, as illustrated in Figure S21 (SI section). It was possible to perform the manual annotation of fifteen Amaryllidaceae alkaloids from diverse nuclei (Table S2, SI section).

The ion of *m/z* 332 at a $t_R$ equal to 10.32 min was annotated as *O*-methyllycorenine. This was not previously grouped together with the standard because it presented only three fragment ions in the molecular network.

Alkaloids of the galanthamine-type skeleton were also annotated in the network of unique nodes. The ion of *m/z* 290 was designated to lycoramine, found only in the wild species *I. amancaes*, which presented abundant fragments at *m/z* 272 and 233 relative to the loss of water and the $C_3H_7N$ unit, and other less abundant ions of *m/z* 215 and 189 referring to the $[M + H - H_2O - C_3H_7N]^+$ ion and the loss of $C_2H_2$ (26 Da), respectively.[36] The *m/z* 306 ion detected among the nodes was annotated as the *N*-oxide of lycoramine, as it exhibits the same fragment ions detected for this mass by Tian *et al*.[44]

The molecular ion at *m/z* 320 was exhaustively searched for in the literature; however, no correspondence was found. It is known that the fragment ions of *m/z* 302 and 288 refer to the neutral losses of water (18 Da) and a $CH_3OH$ unit (32 Da), and their consecutive losses result in the base ion of *m/z* 270 $[M + H - H_2O - CH_3OH]^+$. However, the fragment ions that drew attention were *m/z* 245 and 217, observed in lower abundance. These ions could be formed through the loss of the $C_3H_7N$ and $C_3H_3N$ units, respectively, as found for the alkaloid 3,11-dimethoxylycoramine (*m/z* 334) described by Tian *et al.*[44] The 14 Da difference suggests that a methoxy group was substituted by a hydroxyl group. Based on the fragmentation proposal exhibited by Tian *et al*.,[44] the fragment ion of *m/z* 245 was also found, and due to this, it is suggested that the molecular ion of *m/z* 320 refers to 3-methoxy-11-hydroxylycorenine.[44]

The alkaloids **30**, **32**, **35**, **36**, **39**, **40**, **42**, and **43** (Table S3, SI section) were annotated according to the fragments available in the literature.[34,44,49,50] The elemental composition was verified in the analysis of the raw data. Alkaloid **34** presented fragment ions relative to those observed for the alkaloid hippeastrine. The difference between them (16 Da) suggests that, in this case, it is the alkaloid hippeastrine in its *N*-oxide form.

Other precursor ions, listed in Table S4 (SI section), presenting fragment ions like those previously found, were detected distributed among the unique nodes. However, despite the literature search and the attempt at elucidation, these remain unidentified.

### Relationship between annotations and species

The results obtained from the GNPS platform, combined with the quantitative dataset, enabled the establishment of specific associations between the dereplicated annotations and the plant species responsible for producing the detected metabolites.

The molecular network visualization was configured to display nodes according to their relative intensities in extracts from hybrid and wild species. In hybrid species, the highest intensities corresponded to the alkaloids pseudolycorine, crinine, and hippeastrine. In contrast, in wild species the most abundant alkaloids were crinine, galanthamine, albomaculine, and galanthine.

Galanthamine is of considerable pharmaceutical relevance due to its clinical applicability in the treatment

of Alzheimer's disease. Molecular networking analysis indicated that 69% of the hybrid species were capable of producing galanthamine, with *Amaryllis quito* identified as the major producer. Notably, *A. quito* was the only one responsible for producing the precursor ion at *m/z* 286, assigned to narwedine, a compound scarcely documented in the literature. Therefore, *A. quito* emerges as a promising natural source of both galanthamine and narwedine. According to Eichhorn *et al.*,[51] narwedine is not considered the direct biosynthetic precursor of galanthamine and may exist in equilibrium with it.[51] The exclusive detection of narwedine in *A. quito* suggests the presence of a species-specific biosynthetic route leading to narwedine as either a terminal or intermediate metabolite.

Among the wild species, 30% were also capable of producing galanthamine, with *Hippeastrum papilio* identified as the most productive species across all samples, including both hybrid and wild groups.[52] In addition to galanthamine, *H. papilio* showed high production of albomaculine (*m/z* 346, $t_R$ 9.25 min) and crinine (*m/z* 302, $t_R$ 8.90 min). This species exhibited the highest overall yield among the wild taxa and is considered a promising source of these metabolites, consistent with the findings of Berkov *et al.*[52] Figure S22 (SI section) presents the chromatographic comparison between *A. quito* (black trace) and *H. papilio* (yellow trace). The hybrid species was also identified as the main producer of oduline (*m/z* 286, $t_R$ 6.95 min), an alkaloid belonging to the galanthamine-type structural class.

Lycorine is another alkaloid of substantial pharmacological interest within Amaryllidaceae. The literature reports a broad spectrum of biological activities, including antitumor,[53-56] antiviral (against Dengue virus,[57] Zika virus,[26] and severe acute respiratory syndrome (SARS-CoV-2)[58,59]), anti-*Trichomonas vaginalis*,[22,29] antimalarial,[60] anti-inflammatory,[3] antibacterial,[23] and antifungal[61] properties. The highest lycorine intensities were observed in the hybrid *Amarcrinum*, followed by *Amaryllis clown* and *Amaryllis neon*. *Amarcrinum*, a hybrid between *Amaryllis belladonna* and *Crinum moorei*, produced approximately 1.5-fold higher levels of lycorine compared to the other species and showed lycorine as its third most abundant alkaloid. Another lycorine-type alkaloid, galanthine, was detected in lower abundance in *Amarcrinum* but predominated in *E. amazonica*.

Haemanthidine, a haemanthamine-type alkaloid, was also detected in *Amarcrinum*, as well as in *I. amancaes* and *C. scabrum*. This compound has demonstrated potent activity against the chloroquine-resistant *Plasmodium falciparum* K1 strain ($IC_{50}$ < 1 μg $mL^{-1}$) and against the NF54 strain. It has also shown activity against the trypomastigote forms of *Trypanosoma brucei rhodesiense* and *Trypanosoma cruzi*, highlighting its high therapeutic potential for parasitic diseases.[62]

Among the alkaloids highlighted in the extracts of hybrid species, hippeastrine and crinamidine were particularly prominent. Hippeastrine occurred predominantly in *Amaryllis estrela*, although it was also detected in several other hybrid species at lower intensities within the molecular network. This alkaloid has been reported in the literature to exhibit antiviral, antibacterial, and antifungal activities. However, information regarding its antiparasitic properties remains limited. A recent study[63] identified hippeastrine as a potential inhibitory agent against *T. cruzi*, the etiological agent of Chagas disease.

Crinamidine, a notable alkaloid presents in extracts from both species classifications, was produced by *Eucharis amazonia* and *H. papilio* among the wild taxa, whereas *A. estrela* was the most prominent producer among the hybrid species. Although widely disseminated reports on its antiparasitic activity are lacking, this alkaloid has demonstrated cytotoxic selectivity toward cervical cancer cells in comparison with normal cells. A study conducted by Khumkhrong *et al*.[64] showed that crinamidine is capable of inhibiting the growth of tumor spheroids and inducing apoptosis without causing deoxyribonucleic acid (DNA) damage, which distinguishes it from cisplatin, a reference antineoplastic agent. In addition, this alkaloid also exhibited antiangiogenic activity. Consequently, crinamidine has been suggested as a promising candidate for the treatment and prevention of cervical cancer, highlighting its potential as a bioactive compound in oncological therapy.[64] The species mentioned above, particularly *E. amazonia*, *H. papilio*, and *A. estrela*, emerge as potential sources for the production and isolation of this alkaloid.

The alkaloid candimine, which also exhibits inhibitory activity against *T. vaginalis*[65] and *T. cruzi*,[66] was detected in two species: the wild *Hippeastrum glaucensces* and the hybrid *Amaryllis bogota*. The latter was the major producer, with candimine representing the second most abundant alkaloid in its extract. Pretazetine was the most abundant compound and has been reported to possess antitumor and antiviral properties.[67-69]

Considering the highlighted alkaloids and their reported biological activities, it is plausible that a single compound may be effective against more than one parasite due to structural similarities among target parasites, which may allow interaction with shared molecular targets. Furthermore, some compounds may exert broad mechanisms of action that affect biological processes conserved across multiple parasitic organisms. Nevertheless, it is important to emphasize that the efficacy

of a compound may vary depending on the parasite species and on the specific biological characteristics involved.

The alkaloid albomaculine was found in six hybrid species. The *Amaryllis bingo dobrada* species was identified as the highest producer, and the *H. papilio* wild species exhibited a production level greater than the combined intensity of all six hybrid species. This alkaloid has been evaluated in breast cancer cell lines (Hs578T, MDA-MB-231, MCF7), colon cancer cells (HCT-15), melanoma (SK-MEL-28), and lung cancer cells (A549), as well as against the trypomastigote and amastigote forms of *T. cruzi* and the promastigote and amastigote forms of *Leishmania infantum*.[70,71]

A lack of parasitic activity has also been reported for the alkaloid pseudolycorine. A study conducted by Osorio *et al.*[72] demonstrated significant activity of this alkaloid against the K1 strain of *Plasmodium falciparum*. However, it was inactive against other biological targets, including *T. brucei rhodesiense*, *T. cruzi*, and *Leishmania donovani*.[72] This compound was detected in most extracts of hybrid species and was particularly abundant in *Amaryllis bingo dobrada*, *A. neon*, *A. alaska*, and *A. minerva*. These findings indicate that additional investigations focused on antiparasitic activity may be warranted using species that produce this compound.

### Activity against *Leishmania amazonensis*

The biological activity tests against the promastigote form of the parasitic protozoan *L. amazonensis* and for cytotoxicity in NIH/3T3 fibroblasts were performed as described. The results for all extracts are summarized in Table S5 (SI section).

According to Mota *et al.*,[73] the *in vitro* anti-promastigote activity of plant extracts can be classified according to their $IC_{50}$ values. Extracts exhibiting inhibitory concentration values equal to or lower than 100 μg $mL^{-1}$ are considered active; in the 101-200 μg $mL^{-1}$ range, the activity is considered moderately active; values above 200 μg $mL^{-1}$ indicate that the extracts are categorized as inactive.[73-75] To facilitate the discussion of the results found in this research, the extracts considered active, which presented $IC_{50}$ values below 50 μg $mL^{-1}$ and $CC_{50}$ above 30 μg $mL^{-1}$, and the extract with the poorest activity were selected. These results can be verified in Table 4.

It is observed that 30% of the extracts from wild species presented inhibitory activity against the parasite, being classified among the 5 most potent. The crude extract from the bulbs of the species *I. amancaes* showed the highest inhibitory activity, that is, it demonstrated a better $IC_{50}$ value (1.29 ± 0.9 μg $mL^{-1}$) than the other extracts tested. Furthermore, this extract revealed a low cytotoxicity against NIH/3T3 cells (mouse fibroblasts), highlighting that the sample presents low toxicity to host cells and contains agents selective to the parasite, which is reflected in the selectivity index value (SI = 775.19). The result obtained for this extract reveals a proximity to the values found for the control compound amphotericin B ($IC_{50}$ = 0.04 ± 1.2 μg $mL^{-1}$ and SI = 982.75). These results for the crude extract of *I. amancaes* suggest that the bulbs of this species could be an interesting source of alkaloids with antiparasitic activity.

**Table 4.** Results of $IC_{50}$, $CC_{50}$, and selectivity index of the samples tested on *L. amazonensis* promastigote forms and NIH/3T3 cells

| Sample | $IC_{50}$ promastigote / (μg $mL^{-1}$) | $CC_{50}$ NIH/3T3 / (μg $mL^{-1}$) | SI | SD $IC_{50}$ promastigote | SD $CC_{50}$ NIH/3T3 |
|---|---|---|---|---|---|
| *Ismene amancaes* | 1.29 | > 1000 | 775.19 | –0.9 | nd |
| *Eucharis amazonica* | 16.94 | 73.16 | 4.32 | –1.2 | –1.2 |
| *Amaryllis exposure* | 17.11 | > 1000 | 58.45 | –1.2 | nd |
| *Amarcrinum* | 19.60 | 48.79 | 2.49 | –1.2 | –1.5 |
| *Crinum scabrum* | 23.86 | 50.97 | 2.14 | –1.2 | –1.4 |
| *Amaryllis clown* | 26.68 | > 1000 | 37.48 | –0.8 | nd |
| *Amaryllis barbados* | 33.38 | > 1000 | 29.96 | –1.3 | nd |
| *Amaryllis ferrari* | 40.46 | > 1000 | 24.72 | –0.9 | nd |
| *Amaryllis intokazie* | 40.77 | > 1000 | 24.53 | –1.1 | nd |
| *Amaryllis estrela* | 45.77 | > 1000 | 21.85 | –1.2 | nd |
| *Amaryllis celica* | 46.65 | > 1000 | 21.44 | –1.0 | nd |
| *Hippeastrum glaucescens* | > 1000 | > 1000 | nd | nd | nd |
| ANFB | 0.04 | 39.31 | 982.75 | –1.2 | –0.6 |

$IC_{50}$: minimum inhibitory concentration of 50% in promastigote cells; $CC_{50}$: minimum cytotoxic concentration in NIH/3T3 cells; SI: selectivity index obtained by the ratio between $CC_{50}$ and $IC_{50}$; SD: standard deviation; ANFB: amphotericin B (in μM); nd: not detected.

Through evaluation by UHPLC-ESI(+)MS/MS and molecular network analysis, it was possible to detect nine ions related to Amaryllidaceae alkaloids for the crude extract from the bulbs of *I. amancaes*. Six of these were annotated in the molecular network generated by GNPS, being two of the haemanthamine-type skeleton, haemanthidine (*m/z* 318) and 11-hydroxyvittatine *N*-oxide (*m/z* 304); three of the lycorine-type, goleptine (*m/z* 304), lycorine (*m/z* 288), and 9-norpluviine (*m/z* 274); and two of the galanthamine-type, lycoramine (*m/z* 290) and its *N*-oxide (*m/z* 306). Another five ions were exhaustively searched for in the literature, however, no correspondence was found, with the $[M + H]^+$ ion of *m/z* 350 being present exclusively in this species, albeit as a minor component. The most abundant compound found in this extract was the alkaloid lycoramine in its *N*-oxide form.

Based on the identification of alkaloids from the three species that presented the best selectivity index values mentioned in Table 4, a comparison was conducted between the alkaloids among the species that exhibited the best selectivity indices. It can be summarized that 10 alkaloids were found in the *I. amancaes* sample, while *A. clown* and *A. exposure* presented 8 and 7 alkaloids, respectively. Of these, only lycorine is the common component existing in all three species, in addition to all the others that were listed in Table 4, with the exception of the species *A. estrela*. Some components were found in only two of them, which are two alkaloids (crinamine and *m/z* 268) in *A. exposure* and *A. clown*, and one alkaloid (*m/z* 318) between *I. amancaes* and *A. clown*.

There are few studies concerning the structure-activity relationship between Amaryllidaceae alkaloids and *Leishmania* species. A recent study by Bessa *et al.*[70] showed that the alkaloids haemanthamine, lycorine, and aulicine (crinine-type structure) were active against the promastigote forms of *L. infantum*, exhibiting $IC_{50}$ values equal to 0.6, 9.4, and 11.5 μg $mL^{-1}$, respectively. Among these compounds, haemanthamine was revealed to be the most selective to the parasite; however, it presented a relative cytotoxicity against NCTC cells of 24.7 μM. Despite the toxicity found for this compound, it is worth noting that the alkaloid haemanthamine proved to be 27 times more potent than the control miltefosine ($IC_{50}$ = 16.7 μg $mL^{-1}$) against the promastigote form. Furthermore, it was observed that the same compound presented similar inhibitory activity when tested against the intracellular form, denominated amastigote, of the parasite.[70]

In contrast, according to the authors of this same study, the compounds with a homolycorine-type structure tested against the promastigote form of the *L. infantum* parasite, albomaculine and 7-methoxy-*O*-methylhomolycorine, did not present activity against the parasite.[70] The crude extract from the bulbs of the species *Hippeastrum glauscescens* exhibited the poorest inhibitory activity against the promastigote form of the parasite. According to the analysis of the obtained molecular network, a significant number of alkaloids of the homolycorine nucleus with methoxyl substituents at the C8 and C9 positions are present in the extract in question. Additionally, no alkaloids with antiparasitic activity documented in the literature were found in this same extract.

Studies indicate that the antiparasitic activity found in Amaryllidaceae alkaloids may be linked to the presence of the methylenedioxy group, commonly found at the C8 and C9 positions of these structures, in structures with a tertiary nitrogen.[60,72] Furthermore, it has also been evidenced that molecules that present a tertiary nitrogen without the methyl substituent contribute to the enhancement of antiparasitic activity.[60]

According to the molecular network established in this work, the alkaloids haemanthidine, crinamine, lycorine, and hippeastrine were found in most of the extracts that demonstrated activity against the promastigote form of the parasite. All of these alkaloids present the methylenedioxy group in their structures, corroborating previously described results that suggest this group may contribute to increasing the antiprotozoal activity of these alkaloids. Furthermore, the detection of these alkaloids in the most active samples may indicate a possible synergistic effect between these structures, which are possibly responsible for causing the increase in antiparasitic activity.

## Conclusions

The use of molecular networking emerges as an essential tool for interpreting structural relationships among the alkaloids identified across a large set of samples. FBMN enabled the annotation of 28 alkaloids distributed in six molecular families corresponding to five Amaryllidaceae skeleton types (homolycorine-, haemanthamine-, pretazettine-, lycorine-, and galanthamine-type), in addition to more than 15 alkaloids detected as unique nodes based on spectral similarity and literature data.

The clustering pattern reflected structural similarities, including the formation of two distinct homolycorine-type clusters differentiated by substitution at C2, demonstrating the robustness of the approach for structure-based organization and dereplication in multiple samples.

The inclusion of commercial bulbs, many of them hybrids, increased the sample size and expanded the chemical diversity evaluated, both for alkaloid profiling and antiparasitic activity assessment. Molecular networking

enabled a rapid and less labor-intensive annotation workflow and facilitated the correlation between alkaloid composition and anti-*L. amazonensis* activity. The activity observed for *I. amancaes* may be associated with alkaloids uniquely present in this species or with synergistic interactions among its annotated constituents.

Overall, this integrative approach highlights the chemical diversity within Amaryllidaceae species and identifies promising alkaloid classes as potential targets for further biological and pharmacological investigation.

### Supplementary Information

Supplementary information is available free of charge at http://jbcs.sbq.org.br as PDF file.

### Data Availability Statement

The data presented in this study are available upon request from the corresponding author, as the volume and complexity of the raw mass spectrometry files require specific sharing channels. The data that support the findings of this study are publicly available at Zenodo under the identifier 10.5281/zenodo.18788505 and 10.5281/zenodo.18775387, accessible at: https://doi.org/10.5281/zenodo.18788505 and https://doi.org/10.5281/zenodo.18775387. The FBMN analysis is publicly available at: https://gnps.ucsd.edu/ProteoSAFe/status.jsp?task=588fb452173a4651a06bbd894f38e1b8.

### Acknowledgments

The authors acknowledge the following funding agencies for the fellowships and financial support for this research project: CNPq (grant Nos. 140699/2020-1, 403725/2023-2, 402825/2023-3, 308885/2025-2, 305493/2025-6); FAPES (grant Nos. 991/2022-P, 308/2022-P). This work was partially supported by Programa Iberoamericano de Ciencia y Tecnología para el Desarrollo (CYTED, Red 223RT0140 RENATEC). We extend our appreciation to the Universidade Federal do Espírito Santo (UFES) for providing research infrastructure and the Laboratório de Forense e Petroleômica from the Núcleo de Competências em Química do Petróleo (NCQP-UFES, Brazil) for conducting the analyses. The authors further express their gratitude to the Graduate Program in Chemistry (PPGQUI-UFES, Brazil).

### Author Contributions

A. E. F.: conceptualization, methodology, investigation, formal analysis, data curation, visualization, writing the original draft, and writing (review and editing); M. V. V. L.: methodology, data curation, and writing (review and editing); L. R.; B. A. L.: writing (review and editing); M. R. S. V.: resources; T. B. R.; J. P. A.: methodology and writing (review and editing); W. R.; W. S. B.: conceptualization, visualization, supervision, project administration, and writing (review and editing).

## References

1. Gaudêncio, S. P.; Bayram, E.; Lukić Bilela, L.; Cueto, M.; Díaz-Marrero, A. R.; Haznedaroglu, B. Z.; Jimenez, C.; Mandalakis, M.; Pereira, F.; Reyes, F.; Tasdemir, D.; *Mar. Drugs* **2023**, *21*, 308. [Crossref]
2. Demarque, D. P.; Dusi, R. G.; de Sousa, F. D. M.; Grossi, S. M.; Silvério, M. R. S.; Lopes, N. P.; Espindola, L. S.; *Sci. Rep.* **2020**, *10*, 1051. [Crossref]
3. Atanasov, A. G.; Zotchev, S. B.; Dirsch, V. M.; International Natural Product Sciences Taskforce; Supuran, C. T.; *Nat. Rev. Drug Discovery* **2021**, *20*, 200. [Crossref]
4. Quinn, R. A.; Nothias, L.-F.; Vining, O.; Meehan, M.; Esquenazi, E.; Dorrestein, P. C.; *Trends Pharmacol. Sci.* **2017**, *38*, 143. [Crossref]
5. Nothias, L.-F.; Nothias-Esposito, M.; da Silva, R.; Wang, M.; Protsyuk, I.; Zhang, Z.; Sarvepalli, A.; Leyssen, P.; Touboul, D.; Costa, J.; Paolini, J.; Alexandrov, T.; Litaudon, M.; Dorrestein, P. C.; *J. Nat. Prod.* **2018**, *81*, 758. [Crossref]
6. Aron, A. T.; Gentry, E. C.; McPhail, K. L.; Nothias, L.-F.; Nothias-Esposito, M.; Bouslimani, A.; Petras, D.; Gauglitz, J. M.; Sikora, N.; Vargas, F.; van der Hooft, J. J. J.; Ernst, M.; Kang, K. B.; Aceves, C. M.; Caraballo-Rodríguez, A. M.; Koester, I.; Weldon, K. C.; Bertrand, S.; Roullier, C.; Sun, K.; Tehan, R. M.; Boya, P. C. A.; Christian, M. H.; Gutiérrez, M.; Ulloa, A. M.; Tejeda Mora, J. A.; Mojica-Flores, R.; Lakey-Beitia, J.; Vásquez-Chaves, V.; Zhang, Y.; Calderón, A. I.; Tayler, N.; Keyzers, R. A.; Tugizimana, F.; Ndlovu, N.; Aksenov, A. A.; Jarmusch, A. K.; Schmid, R.; Truman, A. W.; Bandeira, N.; Wang, M.; Dorrestein, P. C.; *Nat. Protoc.* **2020**, *15*, 1954. [Crossref]
7. Wang, M.; Carver, J. J.; Phelan, V. V.; Sanchez, L. M.; Garg, N.; Peng, Y.; Nguyen, D. D.; Watrous, J.; Kapono, C. A.; Luzzatto-Knaan, T.; Porto, C.; Bouslimani, A.; Melnik, A. V.; Meehan, M. J.; Liu, W.-T.; Crüsemann, M.; Boudreau, P. D.; Esquenazi, E.; Sandoval-Calderón, M.; Kersten, R. D.; Pace, L. A.; Quinn, R. A.; Duncan, K. R.; Hsu, C.-C.; Floros, D. J.; Gavilan, R. G.; Kleigrewe, K.; Northen, T.; Dutton, R. J.; Parrot, D.; Carlson, E. E.; Aigle, B.; Michelsen, C. F.; Jelsbak, L.; Sohlenkamp, C.; Pevzner, P.; Edlund, A.; McLean, J.; Piel, J.; Murphy, B. T.; Gerwick, L.; Liaw, C.-C.; Yang, Y.-L.; Humpf, H.-U.; Maansson, M.; Keyzers, R. A.; Sims, A. C.; Johnson, A. R.; Sidebottom, A. M.; Sedio, B. E.; Klitgaard, A.; Larson, C. B.; Boya P, C. A.; Torres-Mendoza, D.; Gonzalez, D. J.; Silva, D. B.; Marques, L. M.; Demarque, D. P.; Pociute, E.; O'Neill, E. C.; Briand, E.; Helfrich, E. J. N.; Granatosky, E. A.; Glukhov, E.; Ryffel, F.; Houson, H.; Mohimani, H.; Kharbush,

J. J.; Zeng, Y.; Vorholt, J. A.; Kurita, K. L.; Charusanti, P.; McPhail, K. L.; Nielsen, K. F.; Vuong, L.; Elfeki, M.; Traxler, M. F.; Engene, N.; Koyama, N.; Vining, O. B.; Baric, R.; Silva, R. R.; Mascuch, S. J.; Tomasi, S.; Jenkins, S.; Macherla, V.; Hoffman, T.; Agarwal, V.; Williams, P. G.; Dai, J.; Neupane, R.; Gurr, J.; Rodríguez, A. M. C.; Lamsa, A.; Zhang, C.; Dorrestein, K.; Duggan, B. M.; Almaliti, J.; Allard, P.-M.; Phapale, P.; Nothias, L.-F.; Alexandrov, T.; Litaudon, M.; Wolfender, J.-L.; Kyle, J. E.; Metz, T. O.; Peryea, T.; Nguyen, D.-T.; VanLeer, D.; Shinn, P.; Jadhav, A.; Müller, R.; Waters, K. M.; Shi, W.; Liu, X.; Zhang, L.; Knight, R.; Jensen, P. R.; Palsson, B. O.; Pogliano, K.; Linington, R. G.; Gutiérrez, M.; Lopes, N. P.; Gerwick, W. H.; Moore, B. S.; Dorrestein, P. C.; Bandeira, N.; *Nat. Biotechnol.* **2016**, *34*, 828. [Crossref]

8. Huo, C.; Nguyen, Q. N.; Alishir, A.; Ra, M.-J.; Jung, S.-M.; Yu, J.-N.; Gwon, H.-J.; Kang, K. S.; Kim, K. H.; *Plants* **2023**, *12*, 3970. [Crossref]
9. Hur, M.; Campbell, A. A.; Almeida-de-Macedo, M.; Li, L.; Ransom, N.; Jose, A.; Crispin, M.; Nikolau, B. J.; Wurtele, E. S.; *Nat. Prod. Rep.* **2013**, *30*, 565. [Crossref]
10. Berkov, S.; Osorio, E.; Viladomat, F.; Bastida, J.; *Alkaloids Chem. Biol.* **2020**, *83*, 113. [Crossref]
11. Bessa, C.; de Andrade, J.; de Oliveira, R.; Domingos, E.; Santos, H.; Romão, W.; Bastida, J.; Borges, W.; *J. Braz. Chem. Soc.* **2016**, *28*, 819. [Crossref]
12. Cole, E. R.; de Andrade, J. P.; Allochio Filho, J. F.; Schmitt, E. F. P.; Alves-Araújo, A.; Bastida, J.; Endringer, D. C.; Borges, W. S.; Lacerda, V.; *Anti-Cancer Agents in Med. Chem.* **2019**, *19*, 707. [Crossref]
13. Gonring-Salarini, K. L.; Conti, R.; de Andrade, J. P.; Borges, B. J. P.; Aguiar, A. C. C.; de Souza, J. O.; Zanini, C. L.; Oliva, G.; Tenorio, J. C.; Ellena, J.; Bastida, J.; Guido, R. V. C.; Borges, W. S.; *J. Braz. Chem. Soc.* **2019**, *30*, 1624. [Crossref]
14. Santos, V.: *Estudo Fitoquímico de Hippeastrum diniz-cruziae Dutilh & Semir e Hippeastrum glaucescens (Mart.) Herb. (Amaryllidaceae)*; PhD Thesis, Universidade Federal do Espírito Santo (UFES), Vitória, Brazil, 2019. [Link] accessed in April 2026
15. Lianza, M.; Verdan, M. H.; de Andrade, J. P.; Poli, F.; de Almeida, L. C.; Costa-Lotufo, L. V.; Cunha Neto, A.; Oliveira, S. C. C.; Bastida, J.; Batista, A. N. L.; Batista, J. M.; Borges, W. S.; *J. Braz. Chem. Soc.* **2020**, *31*, 2135. [Crossref]
16. Nothias, L.-F.; Petras, D.; Schmid, R.; Dührkop, K.; Rainer, J.; Sarvepalli, A.; Protsyuk, I.; Ernst, M.; Tsugawa, H.; Fleischauer, M.; Aicheler, F.; Aksenov, A. A.; Alka, O.; Allard, P.-M.; Barsch, A.; Cachet, X.; Caraballo-Rodriguez, A. M.; da Silva, R. R.; Dang, T.; Garg, N.; Gauglitz, J. M.; Gurevich, A.; Isaac, G.; Jarmusch, A. K.; Kameník, Z.; Kang, K. B.; Kessler, N.; Koester, I.; Korf, A.; Le Gouellec, A.; Ludwig, M.; Martin, H. C.; McCall, L.-I.; McSayles, J.; Meyer, S. W.; Mohimani, H.; Morsy, M.; Moyne, O.; Neumann, S.; Neuweger, H.; Nguyen, N. H.; Nothias-Esposito, M.; Paolini, J.; Phelan, V. V.; Pluskal, T.; Quinn, R. A.; Rogers, S.; Shrestha, B.; Tripathi, A.; van der Hooft, J. J. J.; Vargas, F.; Weldon, K. C.; Witting, M.; Yang, H.; Zhang, Z.; Zubeil, F.; Kohlbacher, O.; Böcker, S.; Alexandrov, T.; Bandeira, N.; Wang, M.; Dorrestein, P. C.; *Nat. Methods* **2020**, *17*, 905. [Crossref]
17. Mohimani, H.; Gurevich, A.; Shlemov, A.; Mikheenko, A.; Korobeynikov, A.; Cao, L.; Shcherbin, E.; Nothias, L.-F.; Dorrestein, P. C.; Pevzner, P. A.; *Nat. Commun.* **2018**, *9*, 4035. [Crossref]
18. Shannon, P.; Markiel, A.; Ozier, O.; Baliga, N. S.; Wang, J. T.; Ramage, D.; Amin, N.; Schwikowski, B.; Ideker, T.; *Genome Res.* **2003**, *13*, 2498. [Crossref]
19. Sumner, L. W.; Amberg, A.; Barrett, D.; Beale, M. H.; Beger, R.; Daykin, C. A.; Fan, T. W.-M.; Fiehn, O.; Goodacre, R.; Griffin, J. L.; Hankemeier, T.; Hardy, N.; Harnly, J.; Higashi, R.; Kopka, J.; Lane, A. N.; Lindon, J. C.; Marriott, P.; Nicholls, A. W.; Reily, M. D.; Thaden, J. J.; Viant, M. R.; *Metabolomics* **2007**, *3*, 211. [Crossref]
20. Reisdorph, N. A.; Walmsley, S.; Reisdorph, R.; *Metabolites* **2019**, *10*, 8. [Crossref]
21. Xiao, H.; Xu, X.; Du, L.; Li, X.; Zhao, H.; Wang, Z.; Zhao, L.; Yang, Z.; Zhang, S.; Yang, Y.; Wang, C.; *Phytomedicine* **2022**, *104*, 154266. [Crossref]
22. Petró-Silveira, B.; Rigo, G. V.; Trentin, D. S.; Macedo, A. J.; Sauer, E.; Alves, E. O.; Tallini, L. R.; Garcia, S. C.; Borges, W. S.; Zuanazzi, J. A. S.; Tasca, T.; *Parasitol. Res.* **2020**, *119*, 2587. [Crossref]
23. Bendaif, H.; Melhaoui, A.; Ramdani, M.; Elmsellem, H.; Douez, C.; El Ouadi, Y.; *Microb. Pathog.* **2018**, *115*, 138. [Crossref]
24. Jia, P.; Sheng, R.; Zhang, J.; Fang, L.; He, Q.; Yang, B.; Hu, Y.; *Eur. J. Med. Chem.* **2009**, *44*, 772. [Crossref]
24. Thomsen, T.; Kewitz, H.; *Life Sci.* **1990**, *46*, 1553. [Crossref]
26. Chen, H.; Lao, Z.; Xu, J.; Li, Z.; Long, H.; Li, D.; Lin, L.; Liu, X.; Yu, L.; Liu, W.; Li, G.; Wu, J.; *Virology* **2020**, *546*, 88. [Crossref]
27. Çitoğlu, G. S.; Acikara, O. B.; Yilmaz, B. S.; Ozbek, H.; *Fitoterapia* **2012**, *83*, 81. [Crossref]
28. Rosa, M. D.; Andrade, J. P.; Costa, A. O.; Conti, R.; Bastida, J.; Borges, W. S.; Furst, C.; *Braz. J. Pharm. Sci.* **2022**, *58*, e20459. [Crossref]
29. Giordani, R. B.; Vieira, P. B.; Weizenmann, M.; Rosemberg, D. B.; Souza, A. P.; Bonorino, C.; de Carli, G. A.; Bogo, M. R.; Zuanazzi, J. A.; Tasca, T.; *Phytochemistry* **2011**, *72*, 645. [Crossref]
30. Lilienfeld, S.; *CNS Drug Rev.* **2002**, *8*, 159. [Crossref]
31. Irwin, R. L.; Smith III, H. J.; *Biochem. Pharmacol.* **1960**, *3*, 147. [Crossref]
32. Heinrich, M.; Teoh, H. L.; *J. Ethnopharmacol.* **2004**, *92*, 147. [Crossref]
33. Ingkaninan, K.; Hazekamp, A.; de Best, C. M.; Irth, H.; Tjaden, U. R.; van der Heijden, R.; van der Greef, J.; Verpoorte, R.; *J. Nat. Prod.* **2000**, *63*, 803. [Crossref]

34. Katoch, D.; Kumar, S.; Kumar, N.; Singh, B.; *J. Pharm. Biomed. Anal.* **2012**, *71*, 187. [Crossref]
35. de Paiva, J.; Souza, A.; Pereira, R.; Ribeiro, P.; Zocolo, G.; de Brito, E.; Pessoa, O.; Canuto, K.; *J. Braz. Chem. Soc.* **2020**, *31*, 1030. [Crossref]
36. Emir, A.; Emir, C.; Bozkurt, B.; Onur, M. A.; Somer, N. U.; Kaya, G. I.; *Braz. J. Pharm. Sci.* **2017**, *53*, e15063. [Crossref]
37. Le, N.-T.-H.; de Jonghe, S.; Erven, K.; Neyts, J.; Pannecouque, C.; Vermeyen, T.; Herrebout, W. A.; Pieters, L.; Tuenter, E.; *Phytochem. Lett.* **2023**, *57*, 156. [Crossref]
38. Ivanov, I.; Berkov, S.; Pavlov, A.; *Biotechnol. Biotechnol. Equip.* **2009**, *23*, 809. [Crossref]
39. Mustafa, N. R.; Rhee, I. K.; Verpoorte, R.; *J. Liq. Chromatogr. Relat. Technol.* **2003**, *26*, 3217. [Crossref]
40. Zhou, X.; Liu, Y.-B.; Huang, S.; Liu, Y.; *J. Huazhong Univ. Sci. Technol. Med. Sci.* **2014**, *34*, 861. [Crossref]
41. Liu, X.; Hong, Y.; He, Q.; Huang, K.; *J. Chromatogr. B: Anal. Technol. Biomed. Life Sci.* **2015**, *974*, 96. [Crossref]
42. Bastida, J.; Lavilla, R.; Viladomat, F.; *Alkaloids Chem. Biol.* **2006**, *63*, 87. [Crossref]
43. Bastida, J.; Berkov, S.; Torras, L.; Pigni, N. B.; Andrade, J. P.; Martinez, V.; Codina, C.; Viladomat, F.; In *Chemical and Biological Aspects of Amaryllidaceae Alkaloids*; Muñoz-Torrero, D., ed.; Transworld Research Network: Trivandrum, India, 2011.
44. Tian, Y.; Zhang, C.; Guo, M.; *Molecules* **2015**, *20*, 21854. [Crossref]
45. de Andrade, J. P.; Pigni, N. B.; Torras-Claveria, L.; Berkov, S.; Codina, C.; Viladomat, F.; Bastida, J.; *J. Pharm. Biomed. Anal.* **2012**, *70*, 13. [Crossref]
46. Fales, H. M.; Wildman, W. C.; *J. Am. Chem. Soc.* **1964**, *86*, 294. [Crossref]
47. Torras-Claveria, L.; Berkov, S.; Viladomat, F.; Bastida, J.; *S. Afr. J. Bot.* **2021**, *136*, 81. [Crossref]
48. Zhang, X.; Huang, H.; Liang, X.; Huang, H.; Dai, W.; Shen, Y.; Yan, S.; Zhang, W.; *Rapid Commun. Mass Spectrom.* **2009**, *23*, 2903. [Crossref]
49. Li, A.; Du, Z.; Liao, M.; Feng, Y.; Ruan, H.; Jiang, H.; *Phytochem. Anal.* **2019**, *30*, 268. [Crossref]
50. Fernández-Galleguillos, C.; Romero-Parra, J.; Puerta, A.; Padrón, J. M.; Simirgiotis, M. J.; *Metabolites* **2022**, *12*, 188. [Crossref]
51. Eichhorn, J.; Takada, T.; Kita, Y.; Zenk, M. H.; *Phytochemistry* **1998**, *49*, 1037. [Crossref]
52. Berkov, S.; Georgieva, L.; Sidjimova, B.; Bastida, J.; *Ind. Crops Prod.* **2022**, *178*, 114619. [Crossref]
53. Roy, M.; Liang, L.; Xiao, X.; Feng, P.; Ye, M.; Liu, J.; *Biomed. Pharmacother.* **2018**, *107*, 615. [Crossref]
54. Lv, F.; Li, X.; Wang, Y.; *BMC Cancer* **2022**, *22*, 873. [Crossref]
55. Wu, S.; Qiu, Y.; Shao, Y.; Yin, S.; Wang, R.; Pang, X.; Ma, J.; Zhang, C.; Wu, B.; Koo, S.; Han, L.; Zhang, Y.; Gao, X.; Wang, T.; Yu, H.; *Front. Pharmacol.* **2018**, *9*, 881. [Crossref]
56. Li, L.; Dai, H.-J.; Ye, M.; Wang, S.-L.; Xiao, X.-J.; Zheng, J.; Chen, H.-Y.; Luo, Y.-H.; Liu, J.; *Cancer Cell Int.* **2012**, *12*, 49. [Crossref]
57. Yonamine, D. K.; Reis, V. E. N.; Feu, A. E.; Borges, W. S.; Cardoso, C. L.; Dinamarco, T. M.; *J. Pharm. Biomed. Anal.* **2024**, *240*, 115935. [Crossref]
58. Jin, Y.-H.; Min, J. S.; Jeon, S.; Lee, J.; Kim, S.; Park, T.; Park, D.; Jang, M. S.; Park, C. M.; Song, J. H.; Kim, H. R.; Kwon, S.; *Phytomedicine* **2021**, *86*, 153440. [Crossref]
59. Ren, P.-X.; Shang, W.-J.; Yin, W.-C.; Ge, H.; Wang, L.; Zhang, X.-L.; Li, B.-Q.; Li, H.-L.; Xu, Y.-C.; Xu, E. H.; Jiang, H.-L.; Zhu, L.-L.; Zhang, L.-K.; Bai, F.; *Acta Pharmacol. Sin.* **2022**, *43*, 483. [Crossref]
60. Sener, B.; Orhan, I.; Satayavivad, J.; *Phytother. Res.* **2003**, *17*, 1220. [Crossref]
61. Silva, L. C.; Correia, A. F.; Gomes, J. V. D.; Romão, W.; Motta, L. C.; Fagg, C. W.; Magalhães, P. O.; Silveira, D.; Fonseca-Bazzo, Y. M.; *Molecules* **2022**, *27*, 2976. [Crossref]
62. Herrera, M. R.; Machocho, A. K.; Nair, J. J.; Campbell, W. E.; Brun, R.; Viladomat, F.; Codina, C.; Bastida, J.; *Fitoterapia* **2001**, *72*, 444. [Crossref]
63. Martinez-Peinado, N.; Cortes-Serra, N.; Torras-Claveria, L.; Pinazo, M.-J.; Gascon, J.; Bastida, J.; Alonso-Padilla, J.; *Parasit. Vectors* **2020**, *13*, 299. [Crossref]
64. Khumkhrong, P.; Piboonprai, K.; Chaichompoo, W.; Pimtong, W.; Khongkow, M.; Namdee, K.; Jantimaporn, A.; Japrung, D.; Asawapirom, U.; Suksamrarn, A.; Iempridee, T.; *Biomolecules* **2019**, *9*, 4940. [Crossref]
65. Giordani, R. B.; Vieira, P. B.; Weizenmann, M.; Rosemberg, D. B.; Souza, A. P.; Bonorino, C.; de Carli, G. A.; Bogo, M. R.; Zuanazzi, J. A.; Tasca, T.; *J. Nat. Prod.* **2010**, *73*, 2019. [Crossref]
66. Ortiz, J. E.; Piñeiro, M.; Martinez-Peinado, N.; Barrera, P.; Sosa, M.; Bastida, J.; Alonso-Padilla, J.; Feresin, G. E.; *Phytomedicine* **2023**, *114*, 154788. [Crossref]
67. Furusawa, E.; Irie, H.; Combs, D.; Wildman, W. C.; *Chemotherapy* **1980**, *26*, 36. [Crossref]
68. Furusawa, E.; Lum, M. K.; Furusawa, S.; *Chemotherapy* **1981**, *27*, 277. [Crossref]
69. Barbosa, E. C.; Alves, T. M. A.; Kohlhoff, M.; Jangola, S. T. G.; Pires, D. E. V.; Figueiredo, A. C. C.; Alves, E. A. R.; Calzavara-Silva, C. E.; Sobral, M.; Kroon, E. G.; Rosa, L. H.; Zani, C. L.; de Oliveira, J. G.; *Virol. J.* **2022**, *19*, 31. [Crossref]
70. Bessa, C. D. P. B.; Feu, A. E.; de Menezes, R. P. B.; Scotti, M. T.; Lima, J. M. G.; Lima, M. L.; Tempone, A. G.; de Andrade, J. P.; Bastida, J.; Borges, W. S.; *Phytomedicine* **2024**, *128*, 155414. [Crossref]

71. Masi, M.; van Slambrouck, S.; Gunawardana, S.; van Rensburg, M. J.; James, P. C.; Mochel, J. G.; Heliso, P. S.; Albalawi, A. S.; Cimmino, A.; van Otterlo, W. A. L.; Kornienko, A.; Green, I. R.; Evidente, A.; *S. Afr. J. Bot.* **2019**, *126*, 277. [Crossref]
72. Osorio, E. J.; Berkov, S.; Brun, R.; Codina, C.; Viladomat, F.; Cabezas, F.; Bastida, J.; *Phytochem. Lett.* **2010**, *3*, 161. [Crossref]
73. Mota, E. F.; Rosario, D. M.; Veiga, A. S. S.; Brasil, D. D. S. B.; Silveira, F. T.; Dolabela, M. F.; *Pharmacogn. Mag.* **2015**, *11*, 601. [Crossref]
74. Veiga, A.; Albuquerque, K.; Corrêa, M. E.; Brigido, H.; Silva e Silva, J.; Campos, M.; Silveira, F.; Santos, L.; Dolabela, M.; *Exp. Parasitol.* **2017**, *175*, 68. [Crossref]
75. Arévalo-Lopéz, D.; Nina, N.; Ticona, J. C.; Limachi, I.; Salamanca, E.; Udaeta, E.; Paredes, C.; Espinoza, B.; Serato, A.; Garnica, D.; Limachi, A.; Coaquira, D.; Salazar, S.; Flores, N.; Sterner, O.; Giménez, A.; *J. Ethnopharmacol*. **2018**, *216*, 120. [Crossref]

*Submitted: December 10, 2025*
*Accepted: April 10, 2026*
*Final version online: May 11, 2026*